Experimental and Computational Multiphase Flow
Vol. 1, No. 3, 2019, 219–229
https://doi.org/10.1007/s42757-019-0010-5

Role of gravity in condensation flow of R1234ze(E) inside horizontal mini/macro-channels

Xin Gu[1], Jian Wen[1], Jin Tian[1], Chaolong Li[1], Huaqing Liu[1], Simin Wang[2] (✉)

1. *Department of Refrigertation and Cryogenics Engineering, School of Energy and Power Engineering, Xi'an Jiaotong University, Xi'an 710049, China*
2. *Department of Process Equipment and Control Engineering, School of Chemical Engineering and Technology, Xi'an Jiaotong University, Xi'an 710049, China*

Abstract

The condensation patterns of R1234ze(E) inside horizontal mini/macro-channels were numerically investigated under normal-gravity and zero-gravity conditions. The gravity effects on condensation heat transfer coefficients, liquid film thickness, film distribution, cross-sectional stream-traces, and liquid-phase velocity were analyzed detailedly. The influence of surface tension on condensation flow was also discussed. The gravity effect on condensation heat transfer coefficients was negligible in mini-channels with D = 1 mm, while was important for D = 2 mm and D = 4.57 mm. The gravity effect can either enhance or weaken the condensation heat transfer coefficient, which was dependent on the tube diameter and vapor quality. The enhancement on heat transfer caused by the gravity was more pronounced at lower vapor quality and mass fluxes with a larger diameter tube. The gravity affected the condensation heat performance through changing the vapor–liquid distribution, rather than the film thickness. The gravity has a great influence on the condensation flow field in both circumferential and axial direction. The surface tension played an important role in heat transfer under zero-gravity condition.

Keywords

condensation
mini/macro-channels
heat transfer
gravity
surface tension

Article History

Received: 4 December 2018
Revised: 8 February 2019
Accepted: 13 February 2019

Research Article

1 Introduction

Condensation inside mini-channels has been widely applied in refrigeration industries, microelectronic system, and space systems for its advantage of high heat transfer rate, compactness, environmental benefits (low refrigerant charge), and withstanding high fluid pressure. The effect of gravity on condensation flow is an important issue when involving the space subsystems (Rankine cycle power conversion, thermal control systems, and advanced life support systems), situations in which tubes need to be tilted and variations of pipe diameter. Knowledge of the gravity effect on condensation flow was crucial as the existing empirical or semi-empirical correlations developed under the normal-gravity condition cannot be directly extrapolated to microgravity conditions (Lips and Meyer, 2012a).

Based on the experimental approach, the gravity effect was discussed through experiments under microgravity conditions or changing the tube inclination under normal-gravity conditions. Lee et al. (2014) experimentally investigated the condensation flow of FC-72 in microgravity achieved by parabolic flights. The heat transfer coefficients decreased along the tube at low mass fluxes, but were enhanced downstream at high mass fluxes for the turbulence and interfacial waviness. They also conducted tests in Lunar gravity and Martian gravity (Lee et al., 2013). The results indicated that the influence of gravity was more pronounced at low mass fluxes. In microgravity, the film was circumferentially uniform in thickness. But for Lunar gravity and Martian gravity, the film was thickened beneath the tube. The team of Meyer (Lips and Meyer, 2012b; Meyer et al., 2014; Ewim et al., 2018) experimentally investigated the effects of inclination angle on condensation heat transfer and characteristic of R134a inside a smooth circular tube. An optimal inclination angle (–15° or –30°) was existed at downward flow, which leaded the highest heat transfer coefficient. They explained that this angle corresponded to a stratified flow with the best trade-off between a low depth of the liquid at the bottom of the tube and a thin falling liquid film at the top of the tube. The effect of inclination is more

✉ smwang@mail.xjtu.edu.cn

Nomenclature

B	Damping factor
C_p	Isobaric specific heat (J·kg^{-1}·K^{-1})
D_h	Hydraulic diameter (m)
E	Specific sensible enthalpy (J·kg^{-1})
g	Gravitational acceleration (m·s^{-2})
G	Mass flux (kg·m^{-2}·s^{-1})
h	Heat transfer coefficient (W·m^{-2}·K^{-1})
h_{lv}	Latent heat of vaporization (J·kg^{-1})
k	Turbulent kinetic energy (m^2·s^{-2})
$\dot{m}$	Mass source due to phase change (kg·m^{-3}·s^{-1})
p	Pressure (Pa)
p_r	Reduced pressure
Pr_t	Turbulent Prandtl number
r	Empirical coefficient (s^{-1})
Re_G	Vapor Reynolds number
Re_L	Liquid Reynolds number
Re_t	Turbulent Reynolds number
S	Modulus of the mean rate-of-strain tensor
T	Temperature (K)
v	Velocity (m·s^{-1})
x	Vapor quality

Greek symbols

α	Volume fraction
σ	Surface tension (N·m^{-1})
σ_k	Turbulent Prandtl number for k
σ_ω	Turbulent Prandtl number for ω
κ_L	Interface surface curvature (m^{-1})
μ	Dynamic viscosity (Pa·s)
μ_t	Turbulent viscosity (Pa·s)
ρ	Density (kg·m^{-3})
λ	Thermal conductivity (W·m^{-1}·K^{-1})
θ	Angular coordinate
δ	liquid film thickness (μm)
ω	Specific dissipation rate of k (s^{-1})

Subscripts

eff	Effective
G	Vapor phase
L	Liquid phase
sat	Saturation

pronounced at lower mass fluxes, lower vapor qualities, and higher saturation temperatures, but decreased with an increase in temperature difference. The team of Akhavan-Behabadi (Akhavan-Behabadi et al., 2007; Mohseni and Akhavan-Behabadi, 2011; Mohseni et al., 2013) conducted an experimental study on the condensation heat transfer characteristic of R134a inside a smooth/microfin tube at different inclinations. The highest heat transfer coefficient can be obtained an inclination angle of 0° at high vapor qualities. But at low vapor qualities, the highest heat transfer coefficient was found at the inclination angle of +30°. They pointed out that for the wavy-annular flow during upward flow, the interfacial turbulences would become the effective parameter for influencing the heat transfer coefficients at low vapor qualities.

With the aid of computational fluid dynamics, a few researchers numerically investigated the influence of gravity on condensation process inside mini/macro-channels. Da Riva and del Col (2011, 2012) numerically investigated the condensation flow of R134a inside a 1 mm horizontal circular tube at steady state. The vapor phase was treated as turbulence while the liquid phase was considered to be laminar. They pointed out that the condensation process was dominated by the gravity at G = 100 kg·m^{-2}·s^{-1}. The stratification due to gravity is shown to enhance the heat transfer. The average heat transfer coefficient in the upper half was found to be three times higher than that in the lower half as the liquid film thickness was much thicker at the bottom for the gravity effect. The team of Li (Zhang and Li, 2016; Li et al., 2017) conducted three-dimensional simulations of condensation inside horizontal tubes at steady state. It was found that the gravity effect was noticeable at lower vapor qualities and mass fluxes for a larger tube diameter. The film thickness decreased with increasing gravity at the upper part of the tube, which increased the average heat transfer coefficients at low mass flux. Wang and Rose (2005, 2006, 2011) developed a theoretical model which included the effect of surface tension, shear stress, and gravity to investigate the condensation flow in mini-channels. They pointed out that the surface tension enhanced the heat transfer at the inlet of the channel for square and triangular section mini-channels, but had a negligible effect for the circular section channel.

Although some studies have been done, it was still far from understanding the gravity effect on condensation flow inside mini or macro-channels. In this paper, three-dimensional simulations about condensation flow of R1234ze(E) under the normal-gravity condition and zero-gravity condition were conducted. The effects of gravity on local condensation heat transfer coefficients, film distribution, film thickness, flow field, and velocity field were analyzed detailedly. This study can be helpful to get a better understanding of the gravity effects on the condensation process.

2 Numerical model

Figure 1 shows the schematic diagram of the geometric model adopted in this paper. The steady-state condensation process of R1234ze(E) inside horizontal circular tubes with diameters ranged from 1 to 4.57 mm was simulated. Both the vapor phase and liquid phase of each refrigerant were considered to be incompressible. The inlet velocity profile of the saturated vapor (T_{sat} = 313 K) including the turbulent kinetic energy and its dissipation rate was obtained by the well-developed single phase flow. A pressure boundary condition was applied at the outlet. The wall was considered to be a smooth non-thickness surface and a no slip wall boundary condition was given. Since in practical application the condensing refrigerant was usually cooled by a secondary fluid, the wall temperature was assumed to be a constant, which was 10 K lower than the saturation temperature. The effect of pressure drop along the tube length on saturation temperature was also neglected. The fluid properties of each refrigerant which were considered to be a function of temperature were derived from the REFPROP 9.0 database (Lemmon et al., 2010).

The computational domain was filled with hexahedral mesh. As shown in Fig. 1, the mesh was refined uniformly near the wall region and the mesh size increased gradually in the radial direction. The distance from the first cell to the wall was 0.8 μm to make sure that the Y^+ was lower than in 1.0. A mesh independence test was conducted at D = 1 mm and G = 600 kg·m^{-2}·s^{-1} in terms of the heat transfer coefficients. In this case, the mesh requirement was the highest because at the same mass flux the velocity magnitude was the largest for the tube with the smallest diameter. The difference was below 0.8% when separately adopting a fine mesh (about 798,000) and a coarse mesh (about 4,700,000). In this paper, the coarse mesh was adopted.

An accurate prediction of flow patterns was necessary for effectively computing the heat transfer coefficient and pressure drop. Recently, Nema et al. (2014) proposed a comprehensive flow regime transition criterion based on the database of Coleman and Garimella (2003). The new criterion widely considered the effects of fluid property, mass flux, vapor quality, and superficial velocities and was expected to be applicable to both macro and mini-channels. Therefore, in this paper, Nema et al.'s model (2014) was adopted to predict the variation of flow regimes inside tubes. As shown in Fig. 2, for brevity, only the transition lines for 1 and 4.57 mm tube were respectively described according to the corresponding criteria. In this paper, the authors mainly focused on investigating the condensation heat transfer characteristic in annular flow regime. As the steady-state mathematical model was not able to deal with the entrainment of droplets in the vapor core, the mist flow was assumed to be annular. Then, during our simulation each tube length was controlled to make sure that the outlet vapor quality was located in the range of annular film flow based on the flow regime map in Fig. 2.

2.1 VOF model

The VOF algorithm has been proved to be an effective way to track the motion of the liquid and vapor interface between two immiscible and incompressible fluids. A continuity equation for the scalar α which represented the volume fraction of any phase beyond the primary in the computational cell was solved. In this paper, the following continuity equation for the volume fraction of the vapor

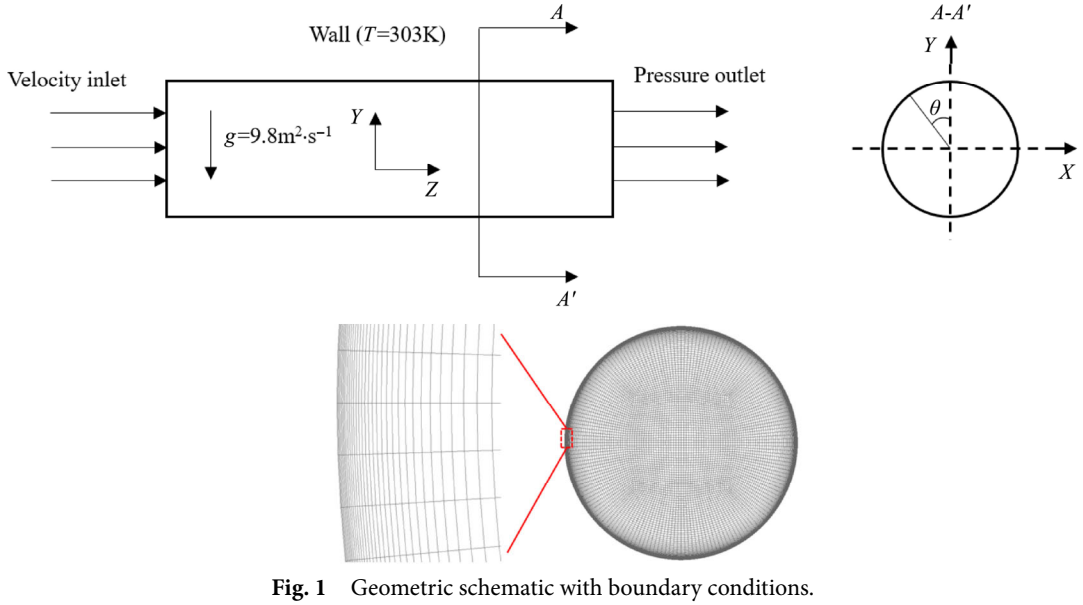

Fig. 1 Geometric schematic with boundary conditions.

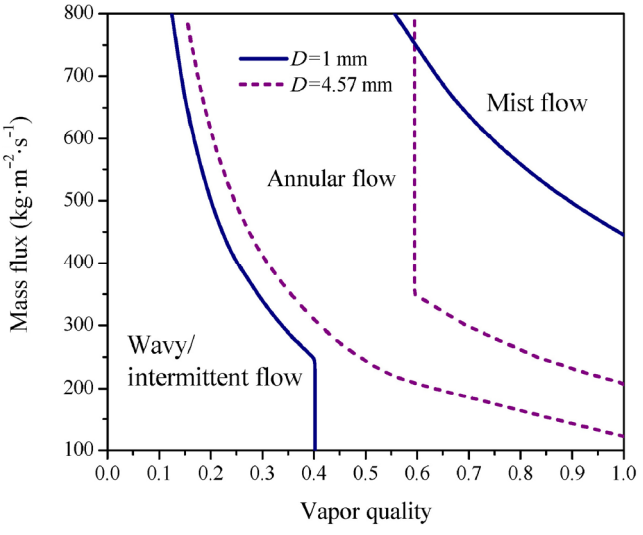

Fig. 2 Flow regime map based on Nema et al. (2014).

phase was computed at steady state.

$$\nabla\cdot(\vec{v}\alpha_{\mathrm{G}})=\frac{\dot{m}_{\mathrm{G}}}{\rho_{\mathrm{G}}} \tag{1}$$

For each control volume, the volume fractions of each phase sum to unity. The liquid phase volume fraction was calculated as follows:

$$\alpha_{\mathrm{L}}+\alpha_{\mathrm{G}}=1 \tag{2}$$

The fluid properties and flow variables were shared by the phases and calculated based on the volume fraction of each phase. The density, viscosity, and thermal conductivity of each cell were calculated by means of an arithmetic mean as follows:

$$\rho=\rho_{\mathrm{L}}\alpha_{\mathrm{L}}+\rho_{\mathrm{G}}\alpha_{\mathrm{G}} \tag{3}$$

$$\mu=\mu_{\mathrm{L}}\alpha_{\mathrm{L}}+\mu_{\mathrm{G}}\alpha_{\mathrm{G}} \tag{4}$$

$$\lambda=\lambda_{\mathrm{L}}\alpha_{\mathrm{L}}+\lambda_{\mathrm{G}}\alpha_{\mathrm{G}} \tag{5}$$

The governing equations including the continuity equation, momentum equation, and energy equation were listed as follows.

Continuity equation:

$$\nabla\cdot(\rho\vec{v})=0 \tag{6}$$

Momentum equation:

$$\nabla\cdot(\rho\vec{v}\vec{v})=-\nabla p+\nabla\cdot[\mu(\nabla\vec{v}+\nabla\vec{v}^{\mathrm{T}})]+\rho\vec{g}+\vec{F} \tag{7}$$

To take into account the effects of surface tension, the continuum surface force (CSF) model proposed by Brackbill et al. (1992) was adopted. Then the force at the surface can be expressed as a volume force and appeared as an additional source term in the momentum equation. The volume force $\vec{F}$ was computed as follows:

$$\vec{F}=\sigma\frac{2\rho\kappa_{\mathrm{L}}\nabla\alpha_{\mathrm{L}}}{\rho_{\mathrm{L}}+\rho_{\mathrm{G}}} \tag{8}$$

The divergence of the unit surface normal at the interface was used to compute the surface curvature.

$$\kappa_{\mathrm{L}}=\nabla\cdot\frac{\nabla\alpha_{\mathrm{L}}}{|\nabla\alpha_{\mathrm{L}}|} \tag{9}$$

Energy equation:

$$\nabla\cdot[\vec{v}(\rho E+p)]=\nabla\cdot(\lambda_{\mathrm{eff}}\nabla T)+h_{\mathrm{lv}}\dot{m}_{\mathrm{L}} \tag{10}$$

$$E=\frac{\alpha_{\mathrm{L}}\rho_{\mathrm{L}}E_{\mathrm{L}}+\alpha_{\mathrm{G}}\rho_{\mathrm{G}}E_{\mathrm{G}}}{\alpha_{\mathrm{L}}\rho_{\mathrm{L}}+\alpha_{\mathrm{G}}\rho_{\mathrm{G}}} \tag{11}$$

$$\lambda_{\mathrm{eff}}=\lambda+\frac{C_p\mu_{\mathrm{t}}}{Pr_{\mathrm{t}}} \tag{12}$$

The Green–Gauss node-based method was applied to compute the gradients. The PRESTO! (PREssure STaggering Option) scheme was used to interpolate the pressure values at the faces. The third order MUSCL scheme was used to discretize the momentum equation, energy equation, and turbulence equations. The pressure–velocity coupling algorithms adopted in this paper was SIMPLE. The Bounded Gradient Maximization (BGM) was employed to obtain sharp interfaces with the VOF model.

2.2 Turbulence model

The turbulence effect is of great importance in the resultant flow pattern and heat transfer performance in the two-phase pipe flow. In this paper, as inspired by Da Riva et al. (2012), the low-Reynolds number form of the Shear Stress Transport (SST) k–ω model was adopted. The damping of turbulence near the interface was also taken into account. The transport equations for the turbulent kinetic energy and its specific dissipation rate were as follows:

$$\frac{\partial}{\partial x_i}(\rho k u_i)=\frac{\partial}{\partial x_j}\left[\left(\mu+\frac{\mu_{\mathrm{t}}}{\sigma_k}\right)\frac{\partial k}{\partial x_j}\right]+\mu_{\mathrm{t}}S^2-\rho\beta^* k\omega \tag{13}$$

$$\frac{\partial}{\partial x_i}(\rho\omega u_i)=\frac{\partial}{\partial x_j}\left[\left(\mu+\frac{\mu_{\mathrm{t}}}{\sigma_\omega}\right)\frac{\partial\omega}{\partial x_j}\right]+\frac{aa^*}{\nu_{\mathrm{t}}}\mu_{\mathrm{t}}S^2-\rho\beta\omega^2+2(1-F_1)\rho\frac{1}{\omega\sigma_{\omega,2}}\frac{\partial k}{\partial x_j}\frac{\partial\omega}{\partial x_j}+S_\omega \tag{14}$$

$$S_\omega=2\alpha_i|\nabla\alpha_i|\Delta n\beta\rho_i\left(\frac{6B\mu_i}{\beta\rho_i\Delta n^2}\right)^2 \tag{15}$$

$$\mu_{\mathrm{t}}=\frac{\rho k}{\omega}\frac{1}{\max\left[\frac{1}{a^*},\frac{SF_2}{a_1\omega}\right]} \tag{16}$$

$$a=\frac{a_\infty}{a^*}\left(\frac{a_0+Re_{\mathrm{t}}/R_\omega}{1+Re_{\mathrm{t}}/R_\omega}\right) \tag{17}$$

$$a^* = a^*_\infty \left(\frac{a^*_0 + Re_t / R_k}{1 + Re_t / R_k} \right) \tag{18}$$

$$Re_t = \frac{\rho k}{\mu \omega} \tag{19}$$

The detailed expressions of empirical closure functions F_1, F_2, β^*, β, and a_∞ can be found in Menter (1994). The empirical constants for the SST k–ω model were set as default values.

2.3 Phase-change model

The most widely used phase-change model derived by Lee (1980) was adopted to simulate the condensation process in this paper. The Lee model (1980) is capable of realizing the phase change process both within the saturated phase and along the interface for condensation, which meet the requirement of simulations in this paper. Therefore, the following equations were added to the governing equations as a source term through the user defined functions.

$$\dot{m}_G = -\dot{m}_L = r\alpha_G \rho_G \frac{(T - T_{sat})}{T_{sat}}, \text{ if } T < T_{sat} \tag{20}$$

$$\dot{m}_G = -\dot{m}_L = r\alpha_L \rho_L \frac{(T - T_{sat})}{T_{sat}}, \text{ if } T > T_{sat} \tag{21}$$

As described in Eq. (20), the phase-change process was mainly driven by the deviation between the cell temperature and saturation temperature. The model assumed that the mass transfer process accompanied by the release or absorption of latent heat occurred at a constant pressure and the interface temperature was equal to T_{sat}. It was easy to understand that if the temperature of a cell was lower than the saturation temperature and $\alpha_G > 0$, the mass flow rate transferred from the vapor phase to the liquid phase would be calculated, but if the cell was full of liquid phase ($\alpha_G = 0$), then no mass transfer was happened. The crucial task when using this model is to find an appropriate value for the coefficient r which was referred to as the mass transfer intensity factor (Sun et al., 2012). It seems that the value of r was dependent on the particular problem and was actually associated with the fluid, geometry, boundary conditions, and even mesh size (Lee et al., 2015). In summary, increasing the value of r would reduce the deviation between the saturation temperature and interface temperature, which is closer to the real situation. However, too large value would cause the convergent difficulty which gives incorrect results. In this paper, this value was determined by a trial-and-error procedure and it finally varied from 4.5×10^5 to 1.5×10^6 s^{-1} according to the specific conditions. On the one hand, the temperature difference between the saturation temperature and interface temperature was limited to 1.0 K, which was considered to be acceptable. On the other hand, the value of r was also verified by comparing the simulated results and experimental data.

3 Results and discussion

3.1 Model validation

To verify the mathematical model in this paper, the simulated heat transfer coefficient of R1234ze(E) were compared with the available experimental data. As shown in Fig. 3, the simulated values of D = 1 mm tube were in good accordance with the experimental data of del Col et al. (2015) with the maximum discrepancy was less than 16.8%. For the D = 4.57 mm tube, for lack of the experimental data of R1234ze(E), the simulation data of R134a were compared with the experimental data of Dobson et al. (1994). As reported by Gu et al. (2018), the condensation heat transfer performance of R1234ze(E) was similar to that of R134a for their similar physical properties. As shown in Fig. 3, the simulation results were in agreement with experimental data of Dobson et al. (1994) with the maximum deviation limited in 5%.

3.2 Effects of gravity on condensation heat transfer coefficients

Condensation heat transfer characteristic of R1234ze(E) was investigated in the case of considering or neglecting the gravity effect. The cross-sectional averaged heat transfer coefficients in horizontal circular tubes were plotted as a function of vapor quality. The gravity effect can either enhance or weaken the condensation heat transfer coefficient, which was dependent on the tube diameter and vapor quality. As shown in Fig. 4(a), for tubes with D = 1 mm and G = 300 kg·m^{-2}·s^{-1}, the HTC was almost coincident with or

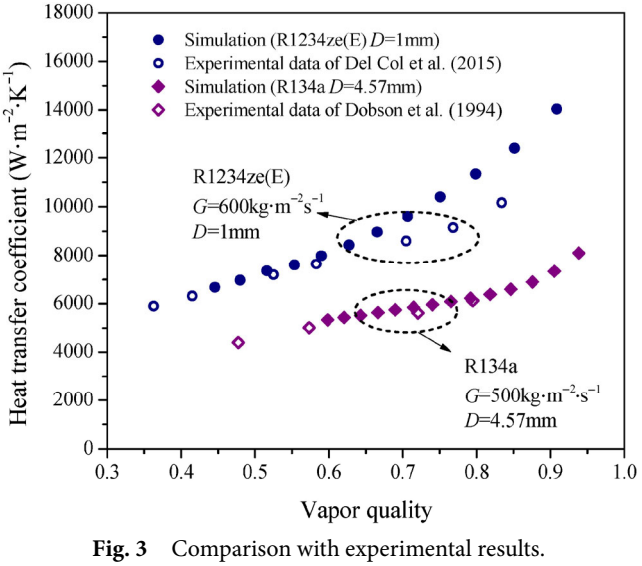

Fig. 3 Comparison with experimental results.

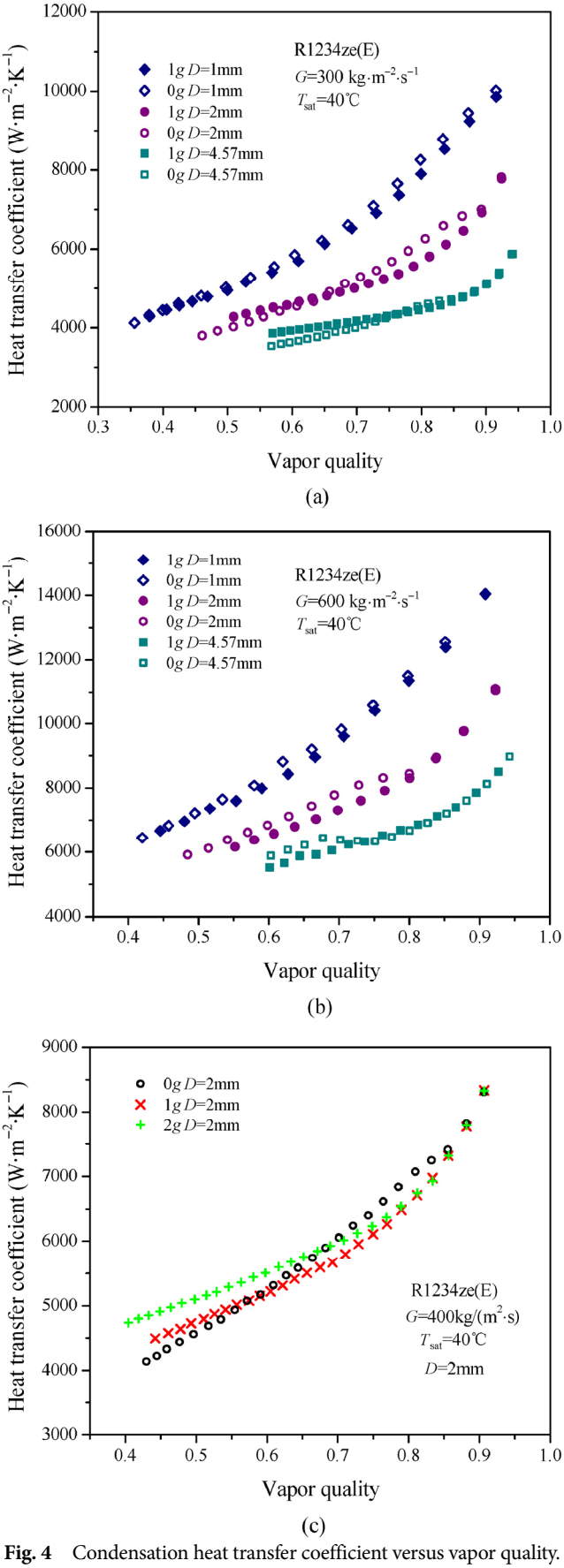

Fig. 4 Condensation heat transfer coefficient versus vapor quality.

without the gravity for vapor qualities decreasing from 1 to 0.35, indicating that the gravity effect was negligible in this case. However, for the D = 2 mm tube, a different behavior can be observed when neglecting the gravity. When the vapor quality was larger than 0.9, there was no difference in heat transfer coefficient. However, for vapor quality varied from 0.9 to 0.65, higher heat transfer coefficient was obtained when neglecting the gravity effect. While the reverse was true for vapor quality lower than 0.65. Similar trend can be observed for 4.57 mm tubes at G = 300 kg·m^{-2}·s^{-1}. The gravity effect decreased with the increase of mass flux. When increasing the mass flux to 600 kg·m^{-2}·s^{-1}, the heat transfer coefficients under normal and zero-gravity condition got closer. The role of shear stress was magnified for the increased mass flux. Instead, the gravity and surface tension effect was somewhat weakened.

Condensation in the circular tube with diameter of 2 mm has been further investigated under double-gravity condition. As shown in Fig. 4(c), by changing the condition from normal-gravity to double-gravity, the heat transfer enhancement caused by the gravity was more noticeable. Compared with the case of zero-gravity condition, the enhancement in heat transfer coefficient caused by the gravity can be observed when x < 0.55 under normal-gravity condition. However, under double-gravity condition it happened when x < 0.65 and the enhancement extent was also greater. The results indicated that the heat transfer enhancement resulted from the gravity would be more important at lower vapor quality or in larger diameter tubes.

3.3 Effects of gravity on average film thickness

The average film thickness defined as the distance between the vapor–liquid interface and tube wall was plotted as a function of vapor quality for better understanding the condensation process in horizontal circular tubes. As illustrated in Fig. 5, the average film thickness obtained with or without the gravity was almost the same for each tube, indicating that the gravity has negligible effect on the film thickness. It can be inferred that the gravity affected the condensation heat performance through changing the vapor–liquid distribution, rather than the film thickness.

3.4 Effects of gravity on liquid film distribution

Figure 6 presents the computed cross-sectional vapor–liquid interface at different vapor qualities for each tube under normal-gravity and zero-gravity conditions. The gravity played an important role in liquid film distribution, which affected the local heat transfer. Such effect increased with the tube diameter but decreased with the increase of vapor quality. As shown in Fig. 6, under the normal-gravity condition, the gravity would pull the liquid phase down to

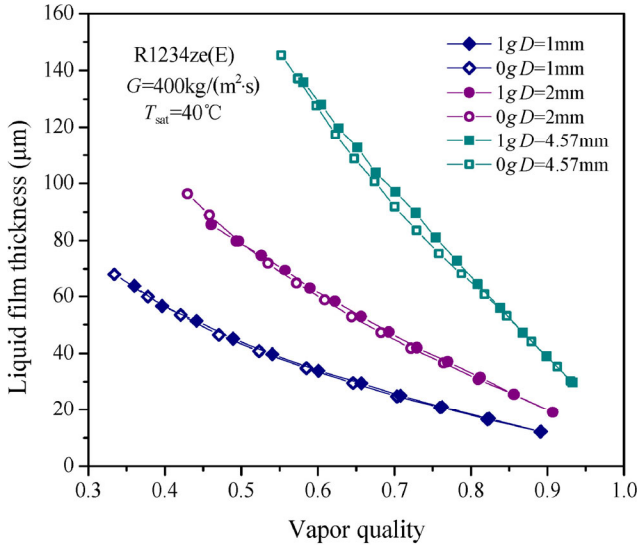

Fig. 5 Average film thickness versus vapor quality.

the bottom of the tube during the condensation process. Therefore, the film thickness at the bottom would become thicker when decreasing the vapor quality. As one can see, the film distribution changed dramatically with the tube diameter. For D = 1 mm, the gravity effect was only noticeable at low vapor quality (x = 0.4). The interface profile displayed a smooth arc shape as the role of surface tension tried to avoid the occurrence of high interfacial curvature for reducing the surface energy. When the diameter increased to 2 mm, for the increased gravity effect and decreased inertia effect, the liquid phase almost all accumulated at the lower half of the tube with generating a very thin liquid film in the upper part of the tube wall. Finally, for D = 4.57 mm, the area of the thin liquid film was magnified and the liquid phase only accumulated at the bottom of the tube. In this case, the gravity played a dominant role in the formation of film distribution. However, under the zero-gravity condition, the liquid film was uniformly distributed along the circumstance for each tube at any vapor quality. In comparison, when considering the gravity effect, the film thickness in the upper part of the tube was reduced, which was beneficial to the heat transfer, while the film thickness in the lower part of the tube was thickened, which increased the thermal resistance there. The difference in film distribution was more noticeable at lower vapor quality or in larger diameter tubes. The trade-off between a thick liquid film at the bottom of the tube and a thin liquid film at the top of the tube affected the local heat transfer performance. At high vapor quality, the liquid film distributed evenly along the circumstance in horizontal tubes. In this case, the increase or decrease in local film thickness in the upper part or lower part of the tube caused by the gravity was relatively close, so that the two effects on local thermal performance can be traded off against each other. However,

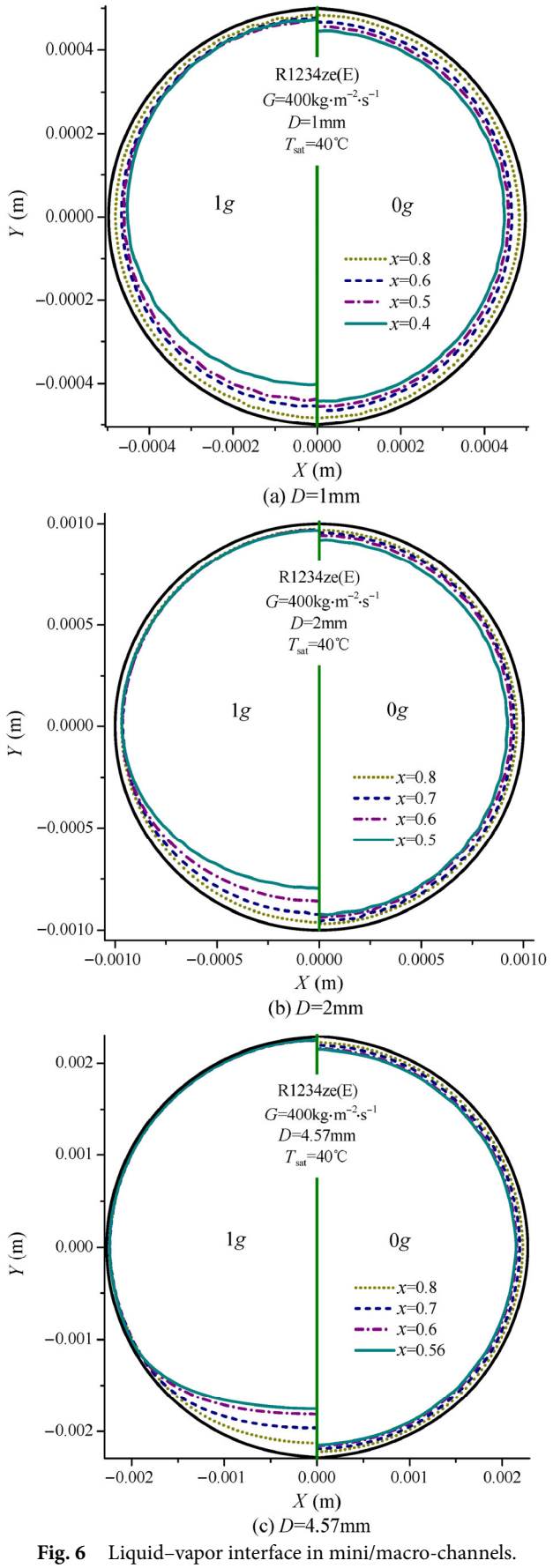

Fig. 6 Liquid–vapor interface in mini/macro-channels.

at low vapor quality, the condensation heat transfer mainly occurred in the thin film area in the upper part of the tube. And the bottom part of the tube had a negligible contribution to the overall heat transfer performance. It was believed that at low vapor quality the heat transfer enhancement in the upper region would prevail over the heat transfer deterioration at the bottom. Therefore, at low vapor quality, the gravity effect on film distribution was overall beneficial to local heat transfer and higher heat transfer coefficients were obtained when considering the gravity ($x < 0.65$ for $D = 2$ mm and $x < 0.75$ for $D = 4.57$ mm)(see Fig. 4). What is more, the enhancement caused by the gravity was considered to be more pronounced at lower vapor quality with a larger diameter tube.

3.5 Effects of gravity on stream-traces

The cross-sectional steam-traces were presented in Fig. 7 to show the gravity effect on the condensation flow field. For each section, only the X and Y components of velocity were considered. The interface line which was in red was also presented to better state the condensation process. Under zero-gravity condition, the streamline started from the center of the tube and moved radially to the interface line where the mass and momentum exchange between the vapor and liquid phase happened. At any vapor quality, the stream-traces were uniformly distributed in the cross-section. However, under normal-gravity condition, it was obvious that the streamline tended to move towards to the upper half of the tube when vapor quality less than 0.755. As discussed before, due to the gravity effect a thin film was formed in the upper part of the tube, which reduced the thermal resistance there. Therefore, the condensation heat and mass transfer process mainly occur in the top portion of the tube. Unlike the case of neglecting the gravity, a tangential velocity of the vapor phase can be observed near the interface line. The condensate in the upside of the tube flowed along the circumference under the pull of the gravity, which gave the vapor phase a downward velocity for the process of the mass and momentum exchange. Under zero-gravity condition, the condensate carried by the shear force owing to the vapor flow only flowed in the axial direction. While under normal-gravity condition, the circumferential motion which varied from the main flow direction was existed. And the movement along the circumference would obstruct the axial flow to some degree. The results indicate that the gravity has a great influence on the condensation flow field in both circumferential and axial directions.

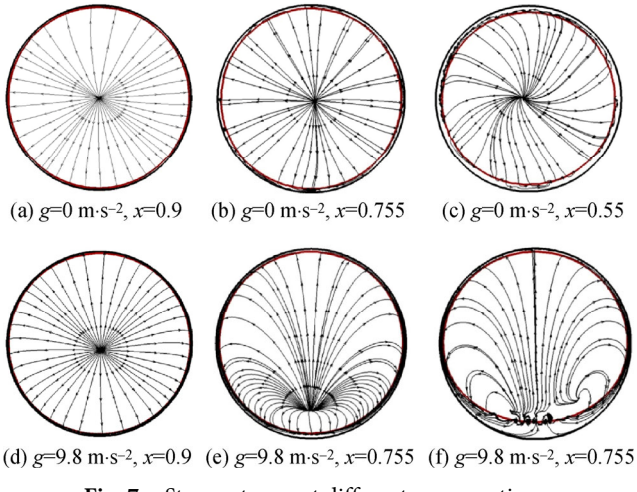

Fig. 7 Stream-traces at different cross-sections.

3.6 Effects of gravity on liquid-phase velocity field

The average liquid-phase velocity as a function of angular coordinate was further plotted in Fig. 8. The gravity had a great influence in the velocity field. The liquid-phase velocity along the circumstance displayed totally different trends when including or not including the gravity. Under the zero-gravity condition, the liquid-phase velocity was almost the same at each circumferential position. In this case, the liquid-phase velocity firstly increased and then decreased with the vapor quality. The condensation flow pattern was dominated by the shear stress at high vapor quality. The vapor-phase velocity was much larger than that of the liquid-phase. Therefore, there was a momentum exchange between the vapor and liquid phase during condensation. As the vapor quality decreasing, the vapor velocity decreased while the liquid velocity increased. However, the viscous frictional resistance between the liquid phase and tube wall would reduce the liquid velocity at low vapor quality. However, under the normal-gravity condition, the liquid phase velocity at the bottom part of the tube was much larger than that at the top part of the tube. The movement along the circumference would influence the liquid-phase velocity at different circumferential positions, especially at the bottom of the tube. Due to the condensate condensed at the top of the tube may flow down to the bottom for the gravity effect, the momentum carried by the condensate at the top of the pipe then transferred to the fluid at the bottom, which increased the liquid phase velocity there. Besides, the circumferential motion of the condensate caused by the gravity prevented the axial flow and thus decreased the axial liquid phase velocity, which was unfavorable for heat exchange as it weakened the heat convection to some extent. Therefore, with reference to the case of zero-gravity condition, including the gravity reduced the liquid-phase velocity in the upper half of the tube but increased the liquid-phase velocity in the bottom part of the tube.

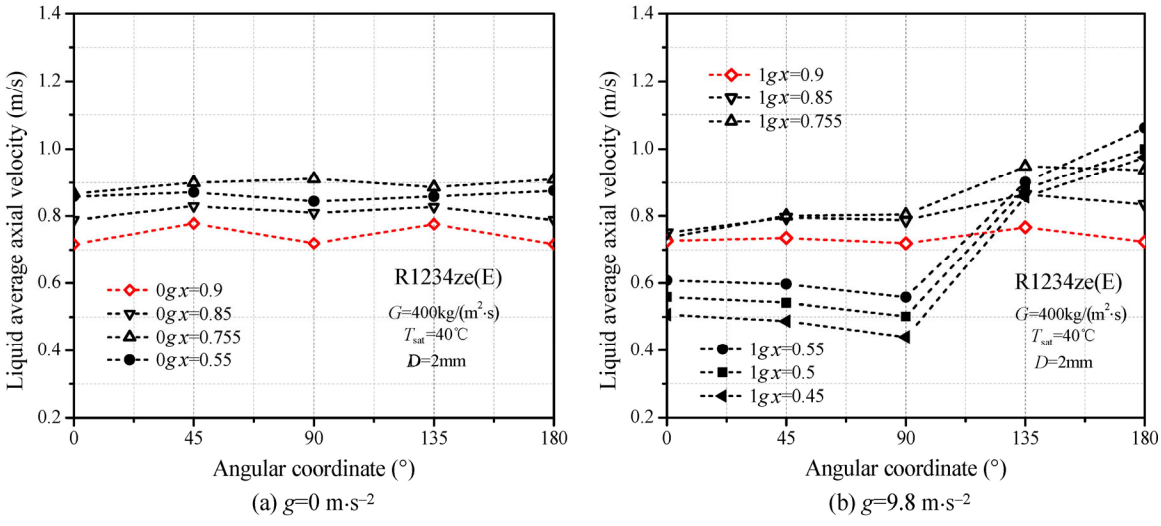

Fig. 8 Axial velocity of liquid phase versus angular coordinate at different vapor qualities.

3.7 Effects of gravity on local heat performance

To illustrate the gravity effect in detail, the local heat transfer coefficient, local liquid film thickness, and local liquid-phase velocity were plotted together as a function of angular coordinate (Fig. 9). Both the local film thickness and local liquid-phase velocity affected the local heat transfer coefficients. For the case of G = 400 kg·m^{-2}·s^{-1}, D = 2 mm, and x = 0.55, without considering the gravity, the local heat transfer coefficient almost unchanged along the circumstance. With considering the gravity, the local heat transfer coefficient overall decreased with the angular coordinate, which was contrary to the film thickness variation. In comparison, the local heat transfer coefficient in the top region was higher when including the gravity. While the reverse was true at the bottom of the tube. An interesting phenomenon was that there existed a certain part of the circumstance (θ from 107.2° to 119.8°) for which the heat transfer coefficient was higher under zero-gravity condition even if the film thickness was thicker in this case. As stated above, the gravity does play a great role in both the local liquid film distribution and liquid-phase velocity during condensation. The thin film area caused by the gravity may increase the local heat transfer coefficient to some extent. However, the axial velocity of the liquid film decreased at the same time, especially in the thin film area, which indicated that the convective heat transfer intensity between the liquid and wall surface was weakened. It seems that the relative importance of film thickness and convective heat transfer intensity determined the final heat transfer performance.

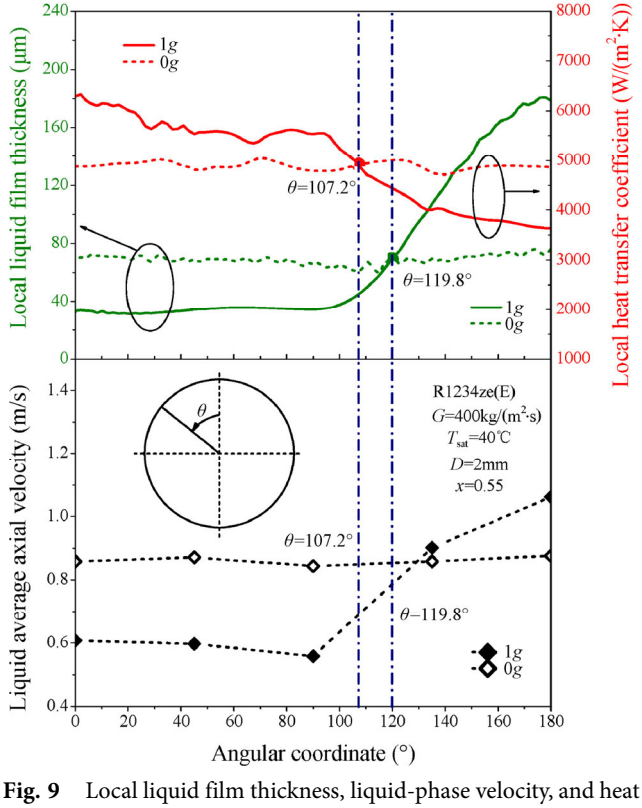

Fig. 9 Local liquid film thickness, liquid-phase velocity, and heat transfer coefficients as a function of angular coordinate.

3.8 Effects of surface tension on condensation heat transfer coefficients

In this paper, simulations have been conducted including and not including the surface tension to investigate the role of surface tension on condensation heat transfer. As shown in Fig. 10, the cross-sectional average heat transfer coefficients with and without surface tension were plotted as a function of vapor quality at G = 300 kg·m^{-2}·s^{-1} and D = 2 mm. The effect of surface tension has been investigated under zero-gravity and normal-gravity conditions. As one can see, the surface tension effect on the condensation heat transfer

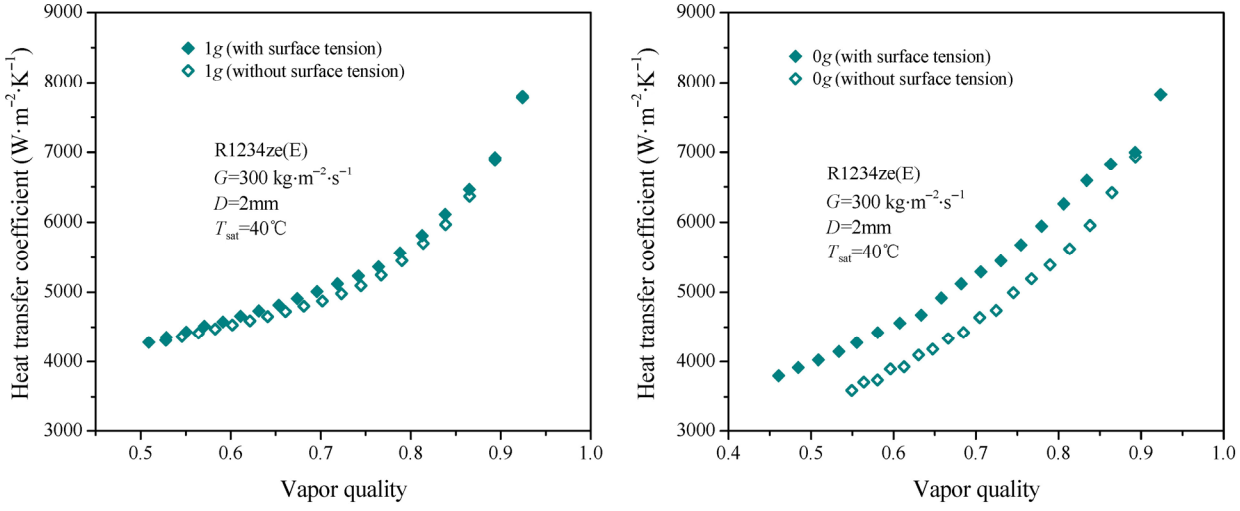

Fig. 10 Effects of surface tension on condensation heat transfer coefficients.

coefficients was almost negligible under the normal-gravity condition. However, under the zero-gravity condition, the surface tension plays an important role in enhancing the heat transfer, which was more obvious at low vapor quality. The enhancement in heat transfer coefficient was around 15% at x = 0.65 and G = 300 kg·m^{-2}·s^{-1}. Under the zero-gravity condition the gravity effect disappeared. Instead, the role of surface tension on heat transfer was enhanced.

4 Conclusions

A numerical study was conducted to investigate the gravity effect on condensation heat transfer characteristic of R1234ze(E) inside horizontal mini/macro-channels. The mass flux ranged from 300 to 600 kg·m^{-2}·s^{-1} and the tube diameter varied from 1 to 4.57 mm. A detailed analysis about the gravity effect on liquid film thickness, film distribution, cross-sectional stream-traces, and liquid-phase velocity was conducted. Besides, the role of surface tension on condensation heat transfer coefficients was also discussed. The main conclusions in this study are summarized as follows. The gravity effect was negligible for D = 1 mm even at G = 300 kg·m^{-2}·s^{-1}, but was of great importance for D = 2 mm and D = 4.57 mm. An enhancement on condensation heat transfer coefficients can be observed at lower mass fluxes and vapor qualities with a larger tube diameter. The gravity has negligible effect on the average film thickness, but played a major role in film distribution. Contrary to the symmetric distribution under zero-gravity condition, a thin film was formed in the upper half of the tube under normal-gravity condition. Similarly, the cross-sectional stream-traces were uniformly distributed under zero-gravity condition, but tended to move towards the upper part of the tube, where the condensation process mainly occurred. Compared with the case of zero-gravity condition, including the gravity reduced the liquid-phase velocity in the upper half of the tube but increased the liquid-phase velocity in the bottom part of the tube. The gravity effects on film distribution and liquid-phase velocity determined the final heat performance. The surface tension effect on condensation heat transfer coefficients were negligible under normal-gravity condition, but played a major role in enhancing heat transfer under zero-gravity condition.

Acknowledgements

This work is supported by the National Natural Science Foundation of China (No. 51676146), for which the authors are thankful.

References

Akhavan-Behabadi, M. A., Kumar, R., Mohseni, S. G. 2007. Condensation heat transfer of R-134a inside a microfin tube with different tube inclinations. *Int J Heat Mass Transfer*, 50: 4864–4871.

Brackbill, J. U., Kothe, D. B., Zemach, C. 1992. A continuum method for modeling surface tension. *J Comput Phys*, 100: 335–354.

Coleman, J. W., Garimella, S. 2003. Two-phase flow regimes in round, square and rectangular tubes during condensation of refrigerant R134a. *Int J Refrig*, 26: 117–128.

Da Riva, E., del Col, D. 2011. Effect of gravity during condensation of r134a in a circular minichannel. *Microgravity Sci Tec*, 23: 87–97.

Da Riva, E., del Col, D. 2012. Numerical simulation of laminar liquid film condensation in a horizontal circular minichannel. *J Heat Transfer*, 134: 051019.

Da Riva, E., del Col, D., Garimella, S. V., Cavallini, A. 2012. The importance of turbulence during condensation in a horizontal circular minichannel. *Int J Heat Mass Transfer*, 55: 3470–3481.

Del Col, D., Bortolato, M., Azzolin, M., Bortolin, S. 2015. Condensation

heat transfer and two-phase frictional pressure drop in a single minichannel with R1234ze(E) and other refrigerants. *Int J Refrig*, 50: 87–103.

Dobson, M. K., Chato, J. C., Hinde, D. K., Wang, S. P. 1994. Experimental evaluation of internal condensation of refrigerants R-134a and R-12. *ASHRAE Transactions*, 100: 744–754.

Ewim, D. R. E., Meyer, J. P., Noori Rahim Abadi, S. M. A. 2018. Condensation heat transfer coefficients in an inclined smooth tube at low mass fluxes. *Int J Heat Mass Transfer*, 123: 455–467.

Gu, X., Wen, J., Wang, C. L., Zhang, X., Wang, S. M., Tu, J. Y. 2018. Condensation flow patterns and model assessment for R1234ze(E) in horizontal mini/macro-channels. *Int J Therm Sci*, 134: 140–159.

Lee, H., Kharangate, C. R., Mascarenhas, N., Park, I., Mudawar, I. 2015. Experimental and computational investigation of vertical downflow condensation. *Int J Heat Mass Transfer*, 85: 865–879.

Lee, H., Mudawar, I., Hasan, M. M. 2013. Experimental and theoretical investigation of annular flow condensation in microgravity. *Int J Heat Mass Transfer*, 61: 293–309.

Lee, H., Park, I., Konishi, C., Mudawar, I., May, R. I., Juergens, J. R., Wagner, J. D., Hall, N. R., Nahra, H. K., Hasan, M. M., MacKey, J. R. 2014. Experimental investigation of flow condensation in microgravity. *J Heat Transfer*, 136: 021502.

Lee, W. H. 1980. A pressure iteration scheme for two-phase flow modeling. In: *Multiphase Transport Fundamentals, Reactor Safety, Applications, Vol. 1*. Veziroglu, T. N. Ed. Washington, DC: Hemisphere Publishing.

Lemmon, E. W., Huber, M. L., McLinden, M. O. 2010. NIST standard reference 23: Reference fluid thermodynamic and transport properties - REFPROP, Version 9.0. Gaithersburg: National Institute of Standard and Technology, Standard Reference Data Program.

Li, W., Zhang, J. Z., Mi, P. F., Zhao, J. F., Tao, Z., Childs, P. R. N., Shih, T. I. P. 2017. The effect of gravity on R410A condensing flow in horizontal circular tubes. *Numer Heat Tr A: Appl*, 71: 327–340.

Lips, S., Meyer, J. P. 2012a. Effect of gravity forces on heat transfer and pressure drop during condensation of r134a. *Microgravity Sci Tec*, 24: 157–164.

Lips, S., Meyer, J. P. 2012b. Experimental study of convective condensation in an inclined smooth tube. Part I: Inclination effect on flow pattern and heat transfer coefficient. *Int J Heat Mass Transfer*, 55: 395–404.

Menter, F. R. 1994. Two-equation eddy-viscosity turbulence models for engineering applications. *AIAA J*, 32: 1598–1605.

Meyer, J. P., Dirker, J., Adelaja, A. O. 2014. Condensation heat transfer in smooth inclined tubes for R134a at different saturation temperatures. *Int J Heat Mass Transfer*, 70: 515–525.

Mohseni, S. G., Akhavan-Behabadi, M. A. 2011. Visual study of flow patterns during condensation inside a microfin tube with different tube inclinations. *Int Commun Heat Mass*, 38: 1156–1161.

Mohseni, S. G., Akhavan-Behabadi, M. A., Saeedinia, M. 2013. Flow pattern visualization and heat transfer characteristics of R-134a during condensation inside a smooth tube with different tube inclinations. *Int J Heat Mass Transfer*, 60: 598–602.

Nema, G., Garimella, S., Fronk, B. M. 2014. Flow regime transitions during condensation in microchannels. *Int J Refrig*, 40: 227–240.

Sun, D. L., Xu, J. L., Wang, L. 2012. Development of a vapor-liquid phase change model for volume-of-fluid method in FLUENT. *Int Commun Heat Mass*, 39: 1101–1106.

Wang, H. S., Rose, J. W. 2005. A theory of film condensation in horizontal noncircular section microchannels. *J Heat Transfer*, 127: 1096–1105.

Wang, H. S., Rose, J. W. 2006. Film condensation in horizontal microchannels: Effect of channel shape. *Int J Therm Sci*, 45: 1205–1212.

Wang, H. S., Rose, J. W. 2011. Theory of heat transfer during condensation in microchannels. *Int J Heat Mass Transfer*, 54: 2525–2534.

Zhang, J. Z., Li, W. 2016. Numerical study on heat transfer and pressure drop characteristics of R410A condensation in horizontal circular mini/micro-tubes. *Can J Chem Eng*, 94: 1809–1819.